(Received 2 June 2025, Accepted 18 July 2025, Scheduled 12 August 2025)

Design of an Ultra-Miniaturized Meandered Patch Antenna for Scalp Applications

Marwah M. Hassooni[1, 2, *], Jabir S. Aziz[3], and Ashwaq Q. Hameed[2]

[1] College of Electrical Engineering, University of Technology, Baghdad, Iraq
[2] Department of Electrical Engineering, College of Engineering, Al-Iraqia University, Baghdad, Iraq
[3] Al-Rafidain University, Baghdad, Iraq

ABSTRACT: This paper introduces the development of an antenna model with a meandering shape in the industrial, scientific, and medical band (i.e., 2.4–2.48 GHz) proposed for biomedical applications. This design is specifically tailored for stimulation applications, where size and form factors are critical. The design of the meandering patch antenna seeks to optimize performance while ensuring compatibility with the unique requirements of stimulation devices. A Rogers RO3010 (loss tangent $= 0.0022$, relative permittivity $= 10.2$) is used in the design as a substrate. The miniaturized antenna ($2.5\,\text{mm} \times 2\,\text{mm} \times 0.12\,\text{mm}$), featuring a 400 MHz bandwidth, was engineered to mitigate detuning effects caused by electronic interference and biological tissue heterogeneity. The smaller dimensions of this antenna not only facilitate easier integration within device structures but also aim to enhance characteristics such as impedance matching and bandwidth, addressing the challenges posed by the confined space within the human body. The proposed antenna also exhibits a -33 dB gain and a lower specific absorption rate (SAR) of 272 W/kg. These attributes position it as a promising solution for biomedical implantation.

1. INTRODUCTION

Implantable medical devices (IMDs) have attracted researchers' interest. Implanted under the skin [1], cochlear [2], retinal [3], heart [4], digestive system [5], etc., they enhance patient life. Efficient implantable medical devices, through progress in biomedical telemetry, are considered the healthiest, implying intertwining with robotic thinking to serve this domain [6]. The antenna is a key component in this device that can pick up vital signals and send them outside the human body to the gateway or caregiver. The stimulated device under the skin of a human head is shown in Fig. 1. The main challenge in the design process is maintaining the best functionality inside a lossy environment, with high bandwidth and gain, and miniaturizing to occupy a small space in IMD [7]. Researchers are persistently striving to address these challenges [8].

Numerous antenna designs have recently been proposed for biotelemetry applications. The authors in [9] present a compact implantable antenna for bio-medical utilization, particularly for scalp implantation. The presented antenna designs achieve two-band properties on the Industrial, Scientific, and Medical (ISM) bands (915 MHz and 2450 MHz) with volumes: 344 mm^3 (System 1) and 406 mm^3 (System 2), with dimensions of the antenna $8 \times 6 \times 0.5 = 24\,\text{mm}^3$ and gain values of -22.8 dBi and -28.5 dBi at a higher and lower frequency bands, and bandwidths are 9.84% and 8.57% at 915 MHz and 2450 MHz, respectively. However, these antennas exhibit considerable size and excessively high specific absorption rate (SAR) values at both frequencies. In [10], the authors propose an implantable ultra-miniaturized antenna that exhibits two-band characteristics in the (915 MHz and 2.45 GHz) industrial, scientific, and medical bands. The antenna has a reduced volume of 9.8 mm^3 ($7\,\text{mm} \times 7\,\text{mm} \times 0.2\,\text{mm}$) and exhibits gain values of -28.04 and -28.94 dBi at a frequency of 915 MHz and -23.01 and -23.06 dBi at 2.45 GHz. Nonetheless, these antennas exhibit considerable size and complicated structure. In [11], an implantable antenna of a two-band circular radiator for skin and scalp implantation is utilized. The proposed antenna covers the 1.395–1.432 GHz Wireless Medical Telemetry Service (WMTS) band and 2.4–2.48 GHz ISM band with a small volume of 18.8 mm^3. The antenna achieves realized peak gains of -24.5 dB and -20.6 dB, respectively. In [12], a miniaturized implantable antenna is designed to work in two frequency bands (ISM) (902–928 MHz) and a midfield band. The volume of 18 mm^3 ($6\,\text{mm} \times 6\,\text{mm} \times 0.5\,\text{mm}$) was compared to the existing works, using a spiral-patch radiator, a shorting strategy, and slots in the ground plane. The results demonstrate bandwidths of 13.4% (871–994 MHz) and 6% (1398–1485 MHz). The maximum realized gain values are -32.8 dBi and -24.8 dBi in the targeted frequency bands. However, the gain is small, and the antenna size is large. The authors in [13] proposed an antenna of self-quadruplexing for a scalp implantable system that takes over a small volume of 22.62 mm^3 ($12\,\text{mm} \times 14.5\,\text{mm} \times 0.13\,\text{mm}$). It exhibits a peak gain of -36.24, -34.78, -31.39, and -30.10 dBi at 168, 433, 915, and 1400 MHz, respectively. The suggested antenna includes four excited semicircular meandered shapes with a usual ground layer. Using four excitation ports, while beneficial for achieving quadruplexing capabilities, adds complexity to the design. In [14], two wideband, low-profile antennas are de-

* Corresponding author: Marwah Malik Hassooni (hassoonimarwa@gmail.com).

signed for implantable communication applications, focusing on their performance as transmitting antennas. The first antenna is intended for implantation within the human body, enabling active signal detection, observation, and transmission. The secondary antenna is an adjacent receiver, facilitating communication with the implanted device. Both antennas operate within the ISM, specifically at 2.4–2.4835 GHz and 5.725–5.875 GHz. The antenna is designed with overall dimensions of (5 mm × 5 mm × 1.02 mm). An ultra-small meander-structured implantable antenna is demonstrated, delivering superior wideband operation at 2450 MHz for medical telemetry applications. This study presents a compact antenna that achieves an ultra-small form factor with a total volume of 0.6 mm^2. This miniaturization is realized through open-ended slots etched into the ground plane and a meandering radiating element. The 400 MHz wideband characteristic exhibits robustness to environmental detuning and IMD-related frequency perturbations.

2. METHODOLOGY

A serpentine structure was created for IMD within a human body tissue at a bio-medical band of frequency of 2.4 GHz, as depicted in Fig. 1. We have used a meandered patch and slots in the bottom layer technique and high permittivity substrate to get the desired results in a small available space, to minimize the size of the design [23, 24]. The consistent width of the patch is etched on a substrate of the dielectric plane with a thickness of 0.12 mm using Rogers RO3010 as a material with a dielectric constant of 10.2. The distance between the metallic strips (0.2 mm in width) is 0.2 mm. The resonant frequency of the meandered radiator was adjusted by varying the metallic strip length. Table 1 presents all the parameters of the model's suggested antenna design.

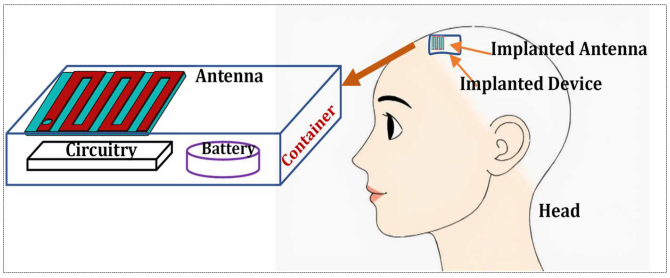

FIGURE 1. Create a generalized illustration of implantable devices.

The progress in the requirements of the implanted systems relies on the offer of ultimate performance to be utilized in the diagnosis, treatment, therapeutic, and monitoring of vital signs, etc. One of the most critical parameters is the miniaturization of electricity in the system. The antenna is a key factor in picking up vital signals and transmitting them outside the human body, and it possesses lossy properties. In this article, a meandered patch antenna is designed with a length of 2 mm and a width of 2.5 mm. The designed antenna contains ground, substrate, and patch. The suggested meander was initially created according to [27]. Initially, the structural parameters of the 2.45 GHz implantable radiator were derived from the given expression.

$$L = \frac{c}{2 \times f\sqrt{\varepsilon_r}} \tag{1}$$

The terms are defined as f (resonant frequency), c (free-space wave propagation speed), L (effective length), and ε_r (resultant relative permittivity). Finally, it is optimized to achieve better outcomes. Thereafter, meandered techniques were applied to reduce the antenna's form factor, enabling deployment in state-of-the-art miniaturized implantable electronics. Introducing apertures to the ground layer increases capacitive effects, facilitating further miniaturization [10].

Signal attenuation occurs during propagation through biological tissues [22], resulting in diminished communication range due to reduced penetration depth. When propagating through lossy media, λ is reduced due to increased dielectric constants, as shown in the equation below [25].

$$\lambda_g = \frac{\lambda}{\sqrt{\varepsilon_r}} \tag{2}$$

Due to the MedRadio band's limitations, including its large size, narrow bandwidth, poor image quality, and low data rates, the industrial, scientific, and medical (ISM) bands are favored for data telemetry [10]. We have used meandered patch and slots in the bottom layer technique and high permittivity substrate to minimize the size of the design. Understanding the design process of the serpentine structure as in Figs. 2(a)–(c), it is considered that the serpentine top layer included six strips with a rectangular shape of length 1.8 mm, width 0.2 mm, and spacing 0.2 mm, which are electrically connected with five connection strips (length 0.2 mm, width 0.2 mm). The spacing among the rectangular strips is 0.2 mm to reduce the impacts of coupling between the strips and exhibit a compact design. 50 Ω coaxial feeding was designed to match the design well with systems at the required frequency.

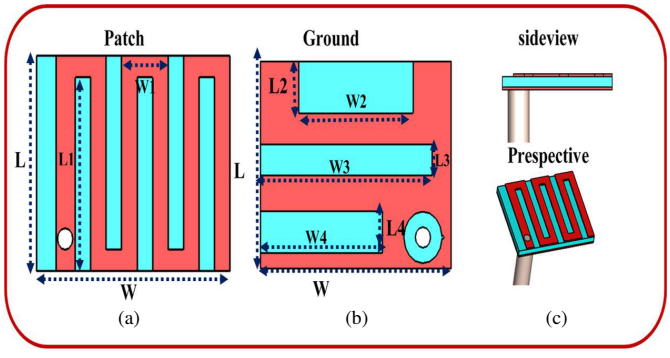

FIGURE 2. The geometrical configuration of the proposed compact antenna of the second model. (a) Radiator structure. (b) Ground plan. (c) Side view.

Table 1 depicts the design parameters of the suggested model. This structure is designed to operate with a particular band, which applies to various applications and accomplishes this target.

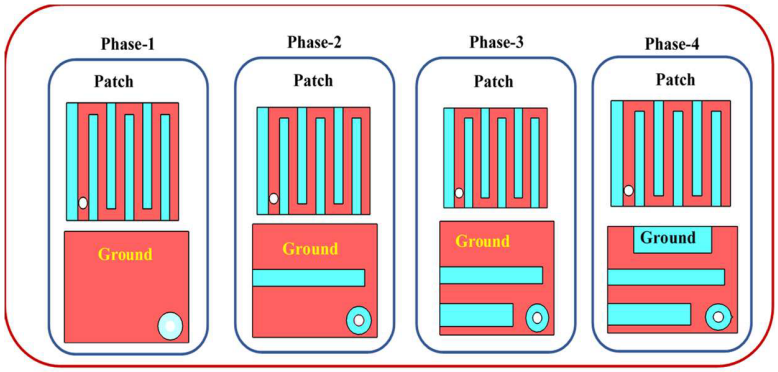

FIGURE 3. Various stages are involved in designing a model.

TABLE 1. Parameters of the design of the suggested model.

Variables	Values (mm)	Variables	Values (mm)
L	2	$L4$	0.4
W	2.5	$W1$	0.6
$L1$	1.8	$W2$	1.5
$L2$	0.5	$W3$	2.25
$L3$	0.3	$W4$	1.6

3. SUGGESTED ANTENNA DESIGN

The suggested model was enhanced in a sequence of phases within the system, as depicted in Fig. 3, with each design phase's related (S_{11}) reflection coefficients across the frequency band from 2.45 GHz to 2.7 GHz. It focuses on identifying the resonant frequency attributes of the model configurations presented in Fig. 4. In phase one, the antenna's initial configuration is assessed, showing a reflection coefficient that begins to drop away from the resonance frequency of 2.45 GHz. This phase provides a baseline for understanding the antenna's inherent characteristics. The performance observed here establishes a reference point for subsequent adjustments. The suggested model operated with a broad bandwidth at 2.7 GHz of 324 MHz. In phase two, a defect was formed in the middle of the ground plane to increase the electrical length, which created a resonance at 2.62 GHz and shifted to the lower frequency. In phase 3, the slot is near the feeding coaxial point; the middle slot is near the bottom edge; and a new resonance is achieved at 2.52 GHz.

Finally, to refine the matching and align the higher operating frequency band with the intended ISM band, a third slot was created near the upper side of the ground plane, and the resonant frequency was set at 2.45 GHz.

4. PARAMETRIC ANTENNA ANALYSIS OF THE MODEL

A parametric analysis of its dimensional parameters was performed to characterize the antenna. We changed various design parameters for the analysis, namely, $L2$, $W3$, $L4$, substrate thickness, and the effect of tissue type.

4.1. Impact of the Variation of $L2$ on the S_{11}

This parametric study used a homogeneous skin phantom of 120 mm × 120 mm × 40 mm of 39.02 dielectric constant and 0.81 conductivity. The variation of the values of $L2$ (0.25 mm, 0.5 mm, and 0.7 mm) in the antenna design significantly impacts the reflection coefficient S_{11}, as evidenced in Fig. 5. Table 2 shows the whole vision of this study, which is the simulation results of the variation of $L2$ on the S_{11}. The value of $L2 = 0.5$ mm was determined to be the best choice based on bandwidth and matching.

TABLE 2. Simulation results of the variation of $L2$ on the S_{11}.

Length $L2$ (mm)	Frequency (GHz)	S_{11} (dB)	BW (MHz)
0.25	2.44	−22	361
0.5	2.44	−25	373
0.7	2.34	−22	356

4.2. Impact of the $W3$ Variation on the S_{11}

Figure 6, corresponding to different values of $W3$ (1.5 mm, 1.75 mm, and 2.25 mm), demonstrates how increasing $W3$ influences the resonance frequency. The curves for $W3 = 1.5$ mm and $W3 = 1.75$ show resonance frequency around 2.45 GHz, but for $W3 = 2.25$ mm, the frequency is resonant at the required frequency. Table 3 shows the results of the variation of $W3$ on the S_{11}.

TABLE 3. Simulation results of the variation of $W3$ on the S_{11}.

Length $W3$ (mm)	Frequency (GHz)	S_{11} (dB)	BW (MHz)
1.5	2.43	−22.2	351
1.75	2.47	−23.23	353
2.25	2.45	−25	375

4.3. Impact of the $L4$ Variation on the S_{11}

The reflection coefficient S_{11} behavior of the antenna model is considerably influenced by the variations in the $L4$ of the slot within the range of 0.1 mm to 0.4 mm, as depicted in Fig. 7. It can be concluded that the resonant frequency moves notably in the direction of the desired band. A better length of $L4$,

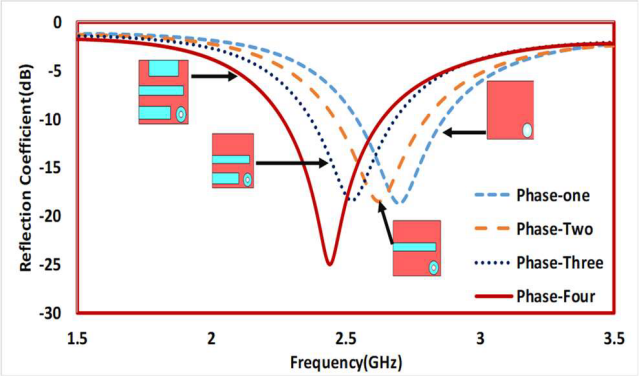

FIGURE 4. S_{11} comparison among the four transit steps of variation in the model.

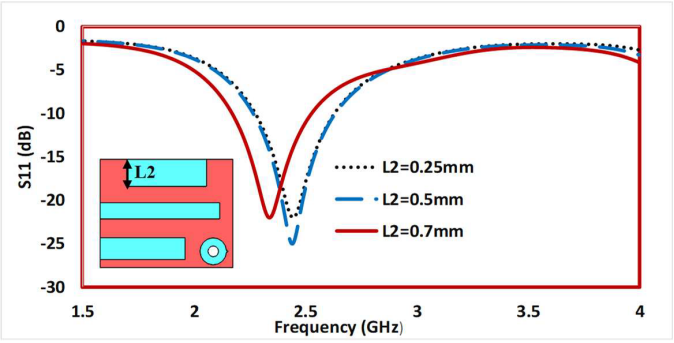

FIGURE 5. Effect of the variation of $L2$ on the S_{11}.

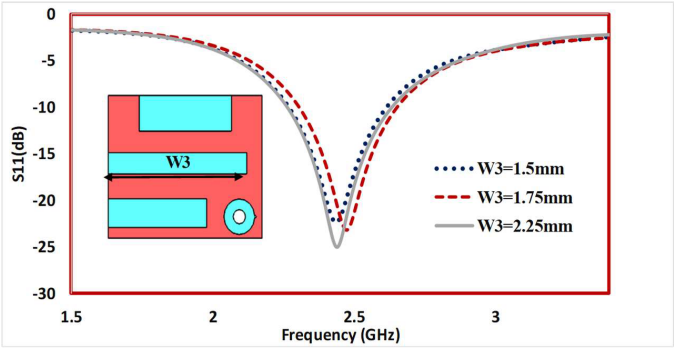

FIGURE 6. Effect of variation $W3$ on the S_{11}.

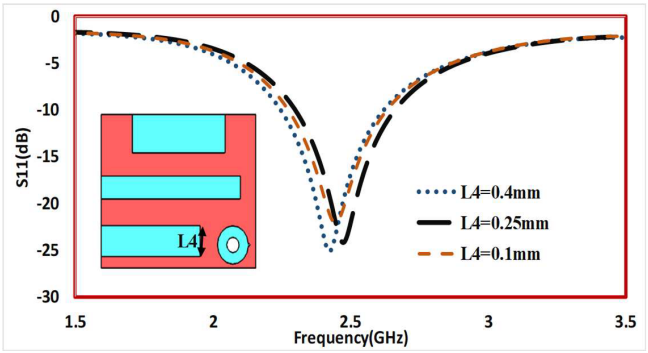

FIGURE 7. Effect of the $L4$ variation on the S_{11} on the model characteristics.

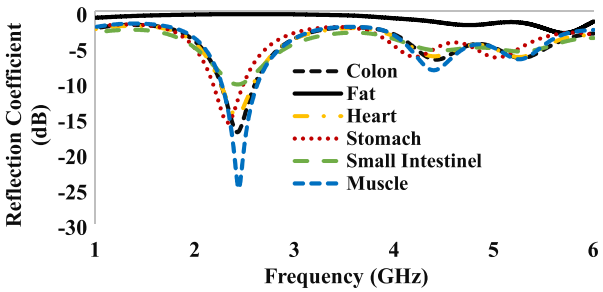

FIGURE 8. Reflection coefficient of the proposed antenna in different scenarios.

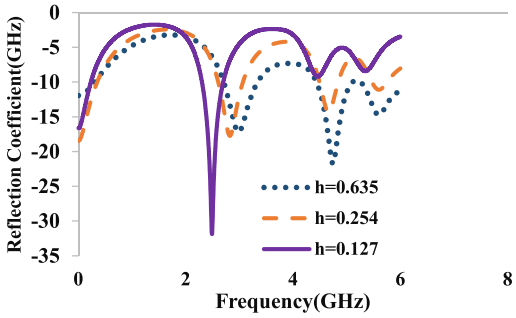

FIGURE 9. The effect of the substrate thickness on the model performance.

considering variations in the slot within the range of 0.1 mm to 0.4 mm, is determined to be 0.4 mm.

4.4. Tissue Type's Effect on Model Performance

The findings regarding the performance of the implantable antenna, as evaluated through simulations in various human phantom tissues, illustrate a reflection coefficient versus frequency relationship. The results demonstrate high suitability for the antenna across different tissue types.

Figure 8 illustrates the implanted antenna's reflection coefficient S_{11} across six biological tissues (fat, heart, stomach, colon, muscle, and intestine), highlighting variations attributed to each medium's distinct electrical properties and lossy nature. While the antenna resonates at approximately 2.4 GHz, the bandwidths at the -10 dB threshold vary significantly across tissues. Notably, fat tissue fails to achieve resonance within this frequency range, whereas the colon tissue exhibits optimal performance, demonstrating the lowest return loss of approximately -17 dB.

4.5. Impact of Substrate Thickness on the Antenna Performance

Figure 9 depicts the reflection coefficient of the model for different substrate thicknesses. The resonance at ISM bands, as evidenced by increasing substrate thickness, shifted the resonant frequency of the antenna toward high frequencies. The

TABLE 4. Simulation results of the variation of substrate thickness on the S_{11}.

Thickness (mm)	Frequency (GHz)	S_{11} (dB)	BW (MHz)
0.635	2.9, 4.7, 5.6	−17.19, −21.72, −15	625, 676, 735
0.254	2.82, 4.66, 5.58	−17.68, −144.3, −11.06	63, 516, 647
0.127	2.47	−38	412

TABLE 5. Maximal value of specific absorption rate for 0.5-watt input power and permitted maximal input powers.

Frequency (GHz)	Tissue structure	Specific Absorption Rate (W/kg)		Maximum provided input power (mW)	
		1 g-Avg	10 g-Avg	1 g-Avg	10 g-Avg
2.45 GHz	Skin	272	28.6	2.94	35

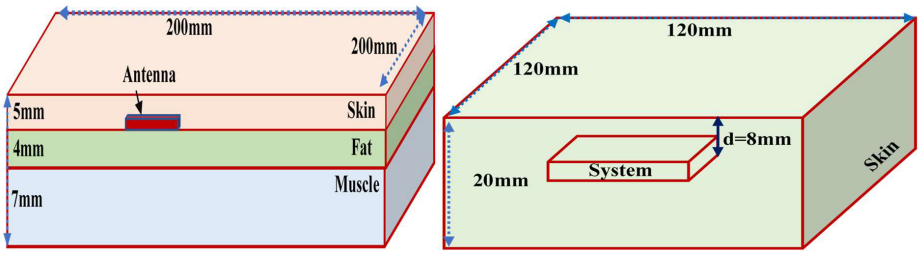

FIGURE 10. The S_{11} in homogeneous and heterogeneous phantoms.

antenna's environment is inside a skin phantom of 8 mm depth. Table 5 explains the simulation results of the variation of substrate thickness on the S_{11}. A thinner substrate decreases the design's overall volume but increases current [23] densities, which reduces bandwidth, as explained in Table 4. The resonant frequency was shifted to a higher frequency value when a thick substrate layer was utilized simultaneously, improving the gain values.

5. ANALYSIS OF ANTENNA IN A HOMOGENEOUS AND HETEROGENEOUS PHANTOM

Figure 10 shows that a phantom dimension of 200 mm × 200 mm × 16 mm was used to implant a meandered antenna in the second scenario of three layers of tissue: skin, fat, and muscle. The simulated S_{11} was not significantly affected, although there were differences in the electrical properties of different human tissues; therefore, the antenna mentioned above is a strong candidate for under-skin applications. Fig. 11 shows the S_{11} in homogeneous and heterogeneous phantoms. S_{11} of heterogeneous in two scenarios shows better matching than a homogeneous phantom.

6. SAR OF MODEL

The calculation of SAR values using a homogeneous skin phantom, characterized by a dielectric constant of 38 and a conductivity of 1.47 S/m to represent skin properties, involves modeling electromagnetic field interactions within a uniform medium that maintains consistent electrical properties across the model [26]. This section presents the specific absorption rate results obtained when the maximum allowable power input was used in the design, illustrating that the specific absorption rate of the antenna can be decreased by reducing the power. The specific absorption rate (SAR) is determined by analyzing the electric field distribution within the phantom by applying the formula [21]:

$$\mathrm{SAR} = \frac{\sigma E^2}{2\rho} \tag{3}$$

where (σ) is the electrical conductivity of the tissue (Siemens/meter), E the electric field (rms), and ρ the density (kg/m^3). Table 5 presents the SAR values obtained at a frequency of 2.48 GHz. When the input power is held at 0.5 W, the SAR values for the 1-gram and 10-gram standards are 272 and 28.6 W/kg, respectively. The power supplied is set to the standard value in Computer Simulation Technology (CST) Microwave Studio software, as other researchers' previous studies have also utilized this standard input power.

Based on these values, we can determine that the maximum amount of allowable power needed to meet the protection standard of 1.6 W/kg for a specific absorption rate of 1 g is 2.94 mW. However, to ensure that the SAR of 10 g does not exceed the safety limit of 2 W/kg, it is necessary to consider an output power of 35 mW. These values satisfy the SAR requirements. The SAR value has been assessed and depicted in Fig. 12.

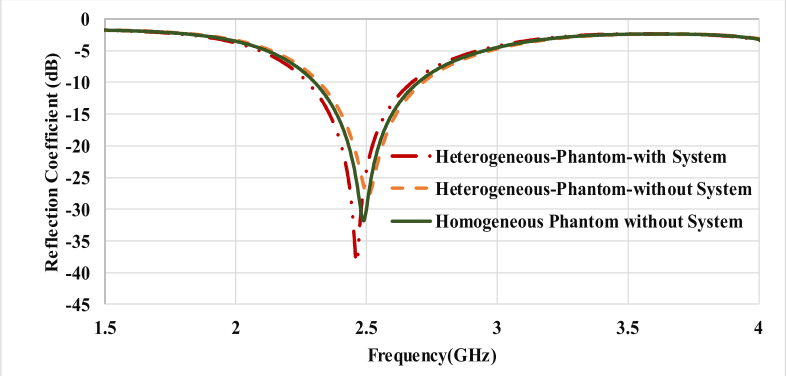

FIGURE 11. Comparison of S_{11} of two scenarios, homogeneous and heterogeneous.

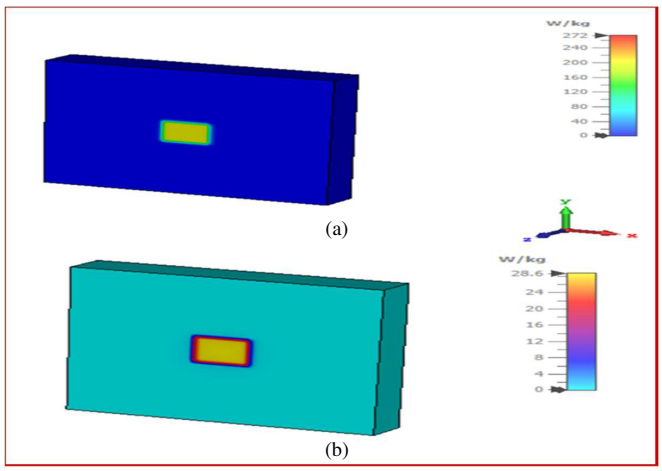

FIGURE 12. (a) Specific Absorption Rate (SAR) of one gram of human tissue at a frequency of 2.45 GHz, (b) SAR of 10 grams of tissue at a frequency of 2.45 GHz.

7. CURRENT DISTRIBUTIONS OF THE MODEL

Figure 13 shows the proposed antenna's current distributions at the resonant frequency. The arrows indicate the direction of surface current flow across the strips. Each strip exhibits a different pattern, suggesting that the current direction changes as it guides through the meandered design. The density of the surface current is noticed to be focused on the excited top layer.

Each strip appears to operate with varying current densities. The regions closer to the edges of the strips show denser current flow. The current distribution suggests that the ground plane is effectively utilized to enhance the overall radiation characteristics of the antenna. Therefore, the current density is noticed to be concentrated at the excited point on the bottom layer.

8. RADIATION PATTERN

Figure 14 presents the simulated polar patterns at the center frequency of the model design (0.245 MHz). The model polar patterns are simulated in two principal planes. The antenna radiation patterns have the same behavior in vertical and horizontal directions. In a heterogeneous phantom, the radiation in the Phi $=0$ plane is 142 degrees, and Phi $=90$ is 174 degrees

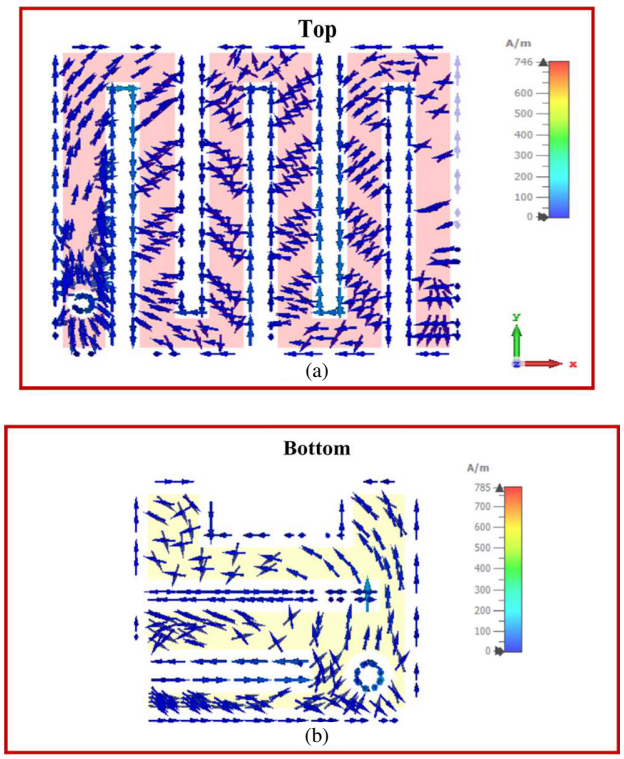

FIGURE 13. A current allocation of the proposed antenna at 2.4 GHz, (a) radiator, (b) ground.

in the skin phantom dimension $=200\,\text{mm} \times 200\,\text{mm} \times 20\,\text{mm}$ and gain $=-33\,\text{dB}$.

9. EXPERIMENTAL SETUP OF MODEL

Figure 15(a) illustrates the fabrication details of the proposed meander-line antenna model, which features a compact size of $2\,\text{mm} \times 2.5\,\text{mm} \times 0.12\,\text{mm}$. The process includes (i) assembly of the SMA connector and coaxial cable, (ii) the top-layer meandered structure, and (iii) the bottom-layer ground plane. Fig. 15(b) illustrates the experimental setup of the model. The container of dimensions $5.4\,\text{mm} \times 12\,\text{mm} \times 30\,\text{mm}$ was used as a dummy stimulated system of thickness 0.2 mm of resin material of $\varepsilon_r = 4$.

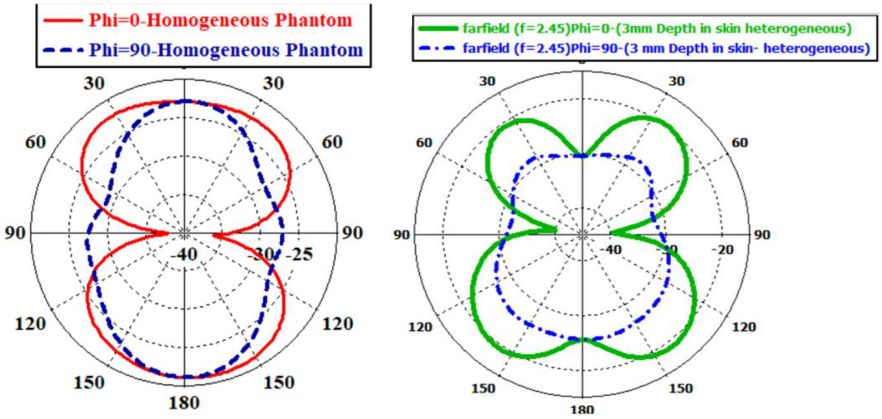

FIGURE 14. Simulated radiation patterns in homogeneous and heterogeneous phantoms.

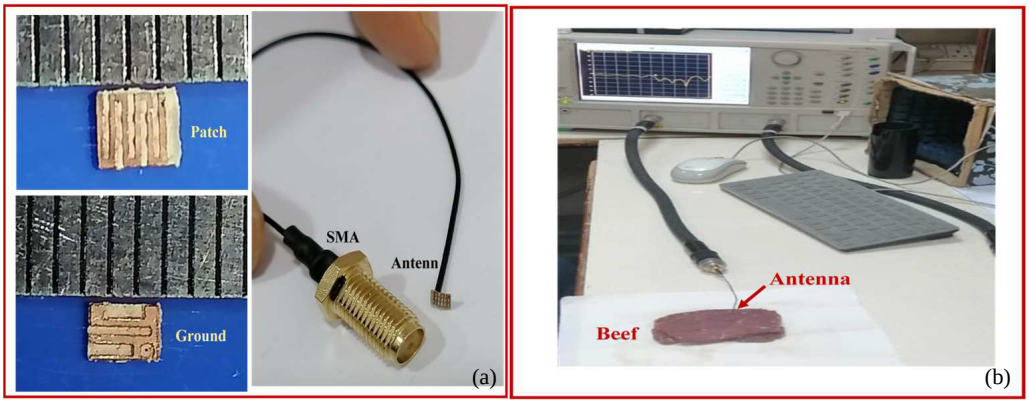

FIGURE 15. (a) The initial steps of the suggested meandered model. (b) Experimental setup of the suggested meandered model.

TABLE 6. Comparison between the characteristics of the suggested antenna and previously published results.

Ref.	Frequency GHz	Size mm^3	Gain (dBi)	BW%	Imp. Dep (mm)
[15]	0.402, 0.915, 1.4, 2.4	$15 \times 15 \times 1.27$	$-30.5/-22.6/-18.2$	4.98	4
[9]	0.915, 2.45	$6 \times 8 \times 0.25$	$-28.5, -22.8$	9.84, 8.57	4
[16]	0.402, 1.6, 2.45	$6 \times 7.5 \times 0.377$	$-30.5, -22.6, -18.2$	36.8, 10.7, 8.9	3
[17]	0.402, 0. 915, 2.4	$32 \times 10 \times 0.25$	$-29.71, -28.7, -20.8$	236.2, 104, 55.4	100
[18]	433, 915	$17.25 \times 8 \times 0.635$	$-28.2, -24.5$	31.9, 21.7	3
[19]	0.402/2.45	$22 \times 23 \times 1.27$	$-36.7, -27.1$	7.4, 6.6	4
[20]	1.400, 1.870, 2.450	$7.2 \times 7.7 \times 0.762$	$-27.4, -21.4, -24.1$	11.5, 19.5, 14.5	3
[12]	0.915, 1.400	$6 \times 6 \times 0.5$	$-32.8, -24.8$	13.4, 6	-
[11]	1.43, 2.44	18.8	$-24.5, -20.6$	6.31, 3.27	3
[21]	5.9	$7 \times 5 \times 0.3$	-32	3.96	2
This model	2.45	$2.5 \times 2 \times 0.12$	-33	16.33	8

10. MEASUREMENTS AND RESULTS OF THE MODEL

The reflection coefficient of the manufactured model antenna was measured and compared with the simulated results. The experimental findings validate the antenna's suitability, aligning its resonances with the designated ISM range 2.4–2.48 GHz bands, as depicted in Fig. 16, and suggest that it is a strong candidate for the use in medically implanted devices (MIDs) due to its ability to perform effectively in the human body environment. The simulated and measured curves align in trend but differ in magnitude, which is common in practical applications due to material properties, fabrication tolerances, and environmental influences. Table 6 presents a performance comparison between our miniaturized wideband antenna and contemporary implantable designs, emphasizing its advancements.

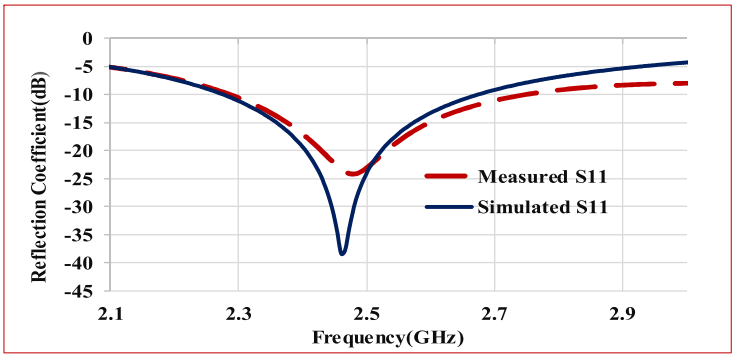

FIGURE 16. Measuring and simulation S_{11} of the proposed model.

11. CONCLUSION

This study introduces a miniaturized ISM-frequency implantable radiator for a scalp stimulation system. The antenna is embedded within a simulated implant assembly, combining electronic circuitry, energy storage units, and a flexible biocompatible antenna structure. The meander-line slots in the radiating element and truncated ground plane aperture prove effective for impedance matching, resonant frequency adjustment, and size reduction. The antenna model, with dimensions of $2.5\,\text{mm} \times 2\,\text{mm} \times 0.12\,\text{mm}$, was designed and simulated using CST Studio Suite®. The antenna was evaluated across diverse implantation environments, including variations in depth and multilayer biological tissue types (e.g., muscle, fat, and skin). The optimized design achieved a gain of $-33\,\text{dB}$ and a bandwidth exceeding 400 MHz.

A prototype was fabricated and experimentally validated through in vivo testing in beef tissue, demonstrating strong agreement between measured results and simulated performance metrics. Experimental results confirm the antenna system's suitability for targeted biotelemetry applications.

REFERENCES

[1] Hassooni, M. M., J. S. Aziz, and A. Q. Hameed, "Ultra-miniaturized spiral antenna for loop recorder implantable device," *Progress In Electromagnetics Research M*, Vol. 132, 21–30, 2025.

[2] Paun, M.-A. and V.-A. Paun, "High-frequency 3-D model for the study of antennas in cochlear implants," *IEEE Transactions on Components, Packaging and Manufacturing Technology*, Vol. 8, No. 7, 1135–1140, 2018.

[3] Kaim, V., B. K. Kanaujia, S. Kumar, H. C. Choi, K. W. Kim, and K. Rambabu, "Electrically small circularly polarized UWB intraocular antenna system for retinal prosthesis," *IEEE Transactions on Biomedical Engineering*, Vol. 69, No. 11, 3504–3515, 2022.

[4] Faisal, F., A. Moulay, M. Chaker, and T. Djerafi, "Efficient wireless power transfer to an ultra-miniaturized antenna for future cardiac leadless pacemaker," in *2024 18th European Conference on Antennas and Propagation (EuCAP)*, 1–4, Glasgow, United Kingdom, 2024.

[5] Li, B., Y. Wang, J. Zhao, and J. Shi, "Ultra-wideband antennas for wireless capsule endoscope system: A review," *IEEE Open Journal of Antennas and Propagation*, Vol. 5, No. 2, 241–255, 2024.

[6] Lafta, W. M., A. A. Alkadhmawee, and M. A. Altaha, "Best strategy to control data on internet-of-robotic-things in heterogeneous networks," *International Journal of Electrical and Computer Engineering (IJECE)*, Vol. 11, No. 2, 1830–1838, 2021.

[7] Kiourti, A. and K. S. Nikita, "Miniature scalp-implantable antennas for telemetry in the MICS and ISM bands: Design, safety considerations and link budget analysis," *IEEE Transactions on Antennas and Propagation*, Vol. 60, No. 8, 3568–3575, 2012.

[8] Yang, Z.-J., S.-Q. Xiao, L. Zhu, B.-Z. Wang, and H.-L. Tu, "A circularly polarized implantable antenna for 2.4-GHz ISM band biomedical applications," *IEEE Antennas and Wireless Propagation Letters*, Vol. 16, 2554–2557, Jul. 2017.

[9] Shah, S. A. A. and H. Yoo, "Scalp-implantable antenna systems for intracranial pressure monitoring," *IEEE Transactions on Antennas and Propagation*, Vol. 66, No. 4, 2170–2173, Apr. 2018.

[10] Faisal, F. and H. Yoo, "A miniaturized novel-shape dual-band antenna for implantable applications," *IEEE Transactions on Antennas and Propagation*, Vol. 67, No. 2, 774–783, Feb. 2019.

[11] Singh, M. S., S. Roy, J. Ghosh, U. Chakraborty, S. Ghosh, and A. Sarkhel, "Design and analysis of compact dual-band antenna system for scalp and skin implantation," *Progress In Electromagnetics Research C*, Vol. 125, 1–13, 2022.

[12] Zhu, L., H. Wang, and Y.-X. Guo, "A dual-band ultra-miniaturized scalp-implantable antenna for in-body bioelectronics," in *2022 IEEE MTT-S International Microwave Biomedical Conference (IMBioC)*, 204–206, Suzhou, China, 2022.

[13] Iqbal, A., M. Al-Hasan, I. B. Mabrouk, and T. A. Denidni, "Self-quadruplexing antenna for scalp-implantable devices," *IEEE Transactions on Antennas and Propagation*, Vol. 72, No. 3, 2252–2260, 2024.

[14] Kamel, Y. A., H. A. Mohamed, H. ELsadek, and H. M. ELhennawy, "RF communication between dual band implantable and on body antennas for biotelemetry application," *Scientific Reports*, Vol. 15, No. 1, 4065, 2025.

[15] Celik, O. F., Y. E. Yamac, and S. C. Basaran, "Compact multi-band implantable antenna designs for versatile in-body applications," *AEU — International Journal of Electronics and Communications*, Vol. 150, 154204, 2022.

[16] Shah, I. A., M. Zada, and H. Yoo, "Design and analysis of a compact-sized multiband spiral-shaped implantable antenna for scalp implantable and leadless pacemaker systems," *IEEE Transactions on Antennas and Propagation*, Vol. 67, No. 6, 4230–4234, 2019.

[17] Basir, A., M. Zada, Y. Cho, and H. Yoo, "A dual-circular-polarized endoscopic antenna with wideband characteristics and

wireless biotelemetric link characterization," *IEEE Transactions on Antennas and Propagation*, Vol. 68, No. 10, 6953–6963, 2020.

[18] Zada, M. and H. Yoo, "Miniaturized dual band antennas for intra-oral tongue drive system in the ISM bands 433 MHz and 915 MHz: Design, safety, and link budget considerations," *IEEE Transactions on Antennas and Propagation*, Vol. 67, No. 9, 5843–5852, 2019.

[19] Liu, Y., Y. Chen, H. Lin, and F. H. Juwono, "A novel differentially fed compact dual-band implantable antenna for biotelemetry applications," *IEEE Antennas and Wireless Propagation Letters*, Vol. 15, 1791–1794, 2016.

[20] Chen, B., Y. Fan, and X. Liu, "Miniaturized wide tri-band antenna for scalp implantable applications," in *2023 International Conference on Microwave and Millimeter Wave Technology (ICMMT)*, 1–3, Qingdao, China, May 2023.

[21] Janapala, D. K., N. Moses, and J. Bhagavathsingh, "Compact size antenna for skin implantable medical devices," *International Journal of Microwave and Wireless Technologies*, Vol. 16, No. 2, 217–226, 2024.

[22] Ullah, S., H. Higgin, M. A. Siddiqui, and K. S. Kwak, "A study of implanted and wearable body sensor networks," in *Agent and Multi-Agent Systems: Technologies and Applications*, Vol. 4953, 464–473, 2008.

[23] Hammood, D. G. and R. T. Hammed, "Performance enhancement of miniaturized dual-band bandpass filter," in *IOP Conference Series: Materials Science and Engineering*, Vol. 1076, No. 1, 012049, 2021.

[24] Thabet, S. F., A. S. Ezzulddin, and O. T. Hamid, "Minimization and optimization in the performance of dual-band BPF by using E-shape microstrip structure," in *2016 8th International Conference on Electronics, Computers and Artificial Intelligence (ECAI)*, 1–6, Ploiesti, Romania, 2016.

[25] Salim, A. J., J. K. Mohammed, H. Al-Saedi, and J. K. Ali, "A proximity-fed multi-band printed antenna for wireless communication applications," *Progress In Electromagnetics Research C*, Vol. 145, 153–165, 2024.

[26] Abduljaleel, H. K., S. Mutashar, and S. K. Gharghan, "Survey of near-field wireless communication and power transfer for biomedical implants," *Engineering and Technology Journal*, Vol. 42, No. 8, 1080–1103, 2024.

[27] Yahya, R. S. and K. Jaehoon, *Implanted Antennas in Medical Wireless Communications*, Synthesis Lectures on Antennas, 2006, https://doi.org/10.2200/S00024ED1V01Y200605-ANT001.